

FlowDet: Unifying Object Detection and Generative Transport Flows

Enis Baty
CVSSP, University of Surrey
e.baty@surrey.ac.uk

C. P. Bridges
SSC, University of Surrey
c.p.bridges@surrey.ac.uk

Simon Hadfield
CVSSP, University of Surrey
s.hadfield@surrey.ac.uk

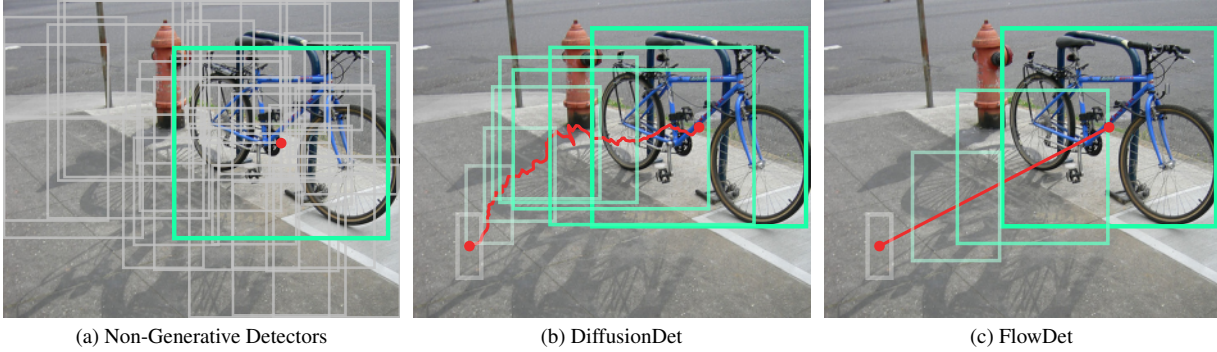


Figure 1. Object detection paradigms: (a) Traditional detectors are limited at inference time, predicting a single set of boxes without the ability to dynamically iterate or transport distant boxes to better predictions. (b) DiffusionDet [10] re-framed detection as a denoising process, enabling generative transport at inference time, at the cost of complex stochastic paths. (c) FlowDet generalises this generative formulation to Conditional Flow Matching, providing shorter, straighter transport paths with greater performance using fewer steps.

Abstract

We present FlowDet, the first formulation of object detection using modern Conditional Flow Matching techniques. This work follows from DiffusionDet, which originally framed detection as a generative denoising problem in the bounding box space via diffusion. We revisit and generalise this formulation to a broader class of generative transport problems, while maintaining the ability to vary the number of boxes and inference steps without re-training. In contrast to the curved stochastic transport paths induced by diffusion, FlowDet learns simpler and straighter paths resulting in faster scaling of detection performance as the number of inference steps grows. We find that this reformulation enables us to outperform diffusion based detection systems (as well as non-generative baselines) across a wide range of experiments, including various precision/recall operating points using multiple feature backbones and datasets. In particular, when evaluating under recall-constrained settings, we can highlight the effects of the generative transport without over-compensating with large numbers of proposals. This provides gains of up to +3.6% AP and +4.2% AP_{rare} over DiffusionDet on the COCO and LVIS datasets, respectively.

1. Introduction

Modern works cast detection as a set prediction problem where a given set of proposals or learnt embeddings are

refined through multi stage heads to an output set of predictions. This enables end-to-end training of the detection model [6, 58], in contrast to classical two-stage approaches [19, 49], significantly improving detection quality. However, at inference time, the performance of these detectors are fixed to the representational budget embedded at train time.

Recently, DiffusionDet [10] proposed an entirely new framing of the detection problem. By casting detection as generative transport from a simple prior, to the data distribution of target boxes, compute can be adjusted dynamically at test time, which has recently gained significant traction in other deep learning domains [54, 63]. Taking more refinement steps or drawing more samples can improve task performance without retraining, at the cost of compute. This also provides flexibility for a given model to be used in either limited compute scenarios (edge inference, mobile devices) or unrestricted for upmost accuracy [24]. Additionally, the generative transport framing removes the need for hand-crafted proposals or separately trained proposal region generation. As such, a simple prior distribution to sample proposals from can be defined and the model learns the transformation to a target set of ground truth instances.

While diffusion has proven to be a strong generative framework, many works seek to reduce the computational burden at inference time [42, 43, 52, 57]. For example, the use of DDIM samplers over the canonical DDPM reduce

the number of steps by about 10-50 \times to produce comparable output quality at inference time. [56] Although significant efforts have been made to improve upon diffusion, contemporary literature has shifted to focus on the very formulation of diffusion to root out transport inefficiency. As such, Conditional Flow Matching (CFM) [37] introduces a generalisation of the diffusion process that further improves the compute-accuracy trade off at integration time.

Conditional Flow Matching is a simulation-free generative modelling framework that trains a time-varying velocity field to move samples from a simple prior to the data distribution. While diffusion samplers trace curved, schedule-induced trajectories, CFM allows for near-linear paths by construction through linear interpolations between prior and target samples as input interpolants during training. Furthermore, instead of random source–target pairings that yield misaligned transport and meandering flows, simple data-aligned priors and transport cost-aware path construction can improve sample efficiency and accuracy at a fixed level of compute. Contrasting diffusion, off-the-shelf ODE solvers provide another angle for precise accuracy-latency control at inference time without schedule tuning.

This work introduces FlowDet, a CFM-based detector generalising the definition of object detection as generative transport in bounding box space. During training, we sample proposal boxes from a simple normal Gaussian distribution and form linear interpolants to ground-truth boxes at randomly sampled timesteps. These interpolants are then used to train the detection head or decoder of our model then to predict the constant velocity flow associated with each interpolant that transports a given bounding box sample from the prior distribution to the target (i.e. ground truth) distribution. At inference time, an arbitrarily sized set of samples are drawn from the prior distribution as proposals. These prior samples are then integrated through the latent flow field embedded within the detection decoder to produce a set of clean bounding box and class label predictions for a given image as shown in Figure 1.

By adopting a generative approach, FlowDet becomes extremely flexible at inference time. Without re-training or fine-tuning, the model can trade-off runtime against precision or recall, by adapting the number of inference steps and source-boxes respectively. With the same ResNet50 [25] backbone we surpass the performance of many strong baselines in detection on the COCO [34] dataset. Specifically compared to DiffusionDet, we achieve +0.1%AP with identical configurations of evaluation boxes and steps and scaling further to a +0.4%AP gain with a higher number of steps.

We summarise our contributions as follows:

- To the best of our knowledge, this work is the first to formally frame detection as a generative transport task using Conditional Flow Matching, generalising the box denoising formulation proposed by DiffusionDet.

- We ablate a broad range of possible data driven priors and matching mechanisms for coupling sources to targets, providing a solid basis for future generative detection approaches to build on.
- We evaluate on standardised benchmarks and backbones, demonstrating FlowDet’s inference time flexibility by operating at various precision/recall tradeoffs without model retraining. Specifically we demonstrate trading compute for recall and accuracy by varying proposal counts and integration steps respectively with a single checkpoint, and achieve notably higher transport efficiency in recall-constrained, few-proposal regimes.

2. Related Work

2.1. Object Detection

Classically, deep object detection approaches formed a two-stage process that relied on classifying hand-crafted region proposals through Selective Search [19, 20, 61] before rapidly progressing to Region Proposal Networks [49]. These two-stage detectors perform well with Region Of Interest (RoI) heads providing strong localisation and robustness at the cost of greater compute through the two distinct proposal and refine stages.

Single-stage “dense” methods adopted direct prediction of boxes from multi-scale feature maps through heuristic anchor grids. These evolved into anchor-free methods treating each location as an object centre, achieving simpler, faster pipelines with competitive accuracy [14, 36, 40, 48, 59].

The rise of the transformer architecture [62] has spawned many works that treat detection as a set prediction problem leading to the development of DETR [6]. Through introducing box-to-box interactions, DETR-family models significantly reduce redundancy within the prediction set and exploit correlations between related objects. Though initially suffering from poor convergence speed and high computational requirements, significant efforts improved both the architectural limitations, [11, 39, 44, 51, 58, 64, 67, 68] and set prediction supervision methods [4, 8, 27, 32, 69].

However, all prior works that rely on dense prediction depend on hand-crafted post-processing such as Non-Maximal Suppression (NMS). Fixed end-to-end methods are also constrained by rigid training time hyper-parameter choices and their behaviour cannot be modulated during deployment. Drawing parallels to image generation, DiffusionDet [10], formulates detection as a denoising diffusion process [26] that iteratively refines noisy boxes to object proposals. In this paper we exploit the same generative formulation for dynamic inference. However, we generalise from basic diffusion denoising to CFM, allowing us to achieve competitive results with very few inference steps.

2.2. Diffusion

Diffusion Denoising Probabilistic Models (DDPM) [26] frame generation as learning to reverse a fixed Gaussian noising process, inspired by non-equilibrium thermodynamics [55]. Models are trained with a noise-prediction objective for noise that gradually corrupts ground truth samples through a Markovian chain in the forward process. The reverse process then starts with pure noise and iteratively “denoises” to produce an output sample that can be influenced with conditioning to guide generation towards specific instance types present in the original training set.

Denoising Diffusion Implicit Models (DDIM) introduce a non-Markovian, deterministic sampler that preserves the original diffusion marginals while enabling few-step generation and exact image-latent inversion providing a valuable speed-quality trade-off [56]. Subsequent work refines schedules, parameterizations, and solvers (e.g., improved diffusion, EDM), but most contemporary systems still build on the DDPM objective with DDIM-style fast samplers for efficient inference and controllable guidance [30, 45].

Although DDIM enables relatively fast sampling, the efficiency of the diffusion process is still the leading challenge in the field. Given the stochastic formulation of the task, the denoising process is computationally expensive and provides poor results with few inference time sampling steps.

2.3. Conditional Flow Matching

Continuous Normalising Flows (CNFs) model generation as the integration of a learned, time-varying flow that transports a simple prior to the data distribution [9, 21, 46]. Conditional Flow Matching (CFM), provides a simulation-free objective to train CNFs by regressing the velocity field along a user-specified probability path. This unifies flow-based and diffusion-style training within a single framework, where diffusion arises as a specific path choice, making diffusion a special case of flow matching [1, 2, 15, 37]. This perspective exposes explicit design levers such as prior distributions, paths, coupling strategies and supports deterministic sampling via standard ODE solvers that allow for an accuracy/compute trade-off chosen at inference time.

Recent work refines the framework in three key areas: path design, coupling, and straight-trajectory training. Optimal-Transport (OT) couplings and mini-batch OT improve alignment between source and target, shortening transport and stabilizing training [5, 60]. Straight-path objectives such as Optimal Flow Matching and Rectified Flow reduce curvature and path length, improving sample efficiency and enabling few-step or even one-step generation without sacrificing fidelity [28, 41]. Conditional variants broaden applicability, with Conditional Variable Flow Matching (CVFM) generalising to continuous conditioning with unpaired data and reflected/variational rectified flows further tighten the train–test gap to improve solver robustness [18, 22, 66].

To the best of our knowledge, this work is the first to generalise the generative detection problem to the broader category of flow-based methods. This enables us to adopt Conditional Flow Matching techniques, preserving the test-time flexibility established by diffusion-based detectors while learning more compact flow fields that require less recursive calls to traverse at inference time.

3. Methodology

3.1. Preliminaries

Conditional Flow Matching (CFM) builds upon the formulation of Continuous Normalizing Flow (CNF), which transform a probability density $p(x)$ via an ordinary differential equation (ODE) $\frac{dx}{dt} = v_\theta(x, t)$ from a simple prior $p_0(x)$ at $t = 0$ to the data distribution $p_1(x)$ at $t = 1$ [9]. In both CNFs and CFM, the time-dependent vector field $v_\theta(x, t)$ is parametrised by a neural network, however the key differences lie in the training of v_θ enabling the scaling of CFM for use in non-trivial settings.

CNFs enable flexible transformations but require computing the log-determinant (trace) of the Jacobian $\frac{\partial v_\theta}{\partial x}$ to track probability densities via the instantaneous change-of-variables formula. This is computationally expensive and typically approximated by stochastic trace estimation, introducing training instability and scalability issues [21, 46].

CFM circumvents this intractability by training a model to regress the underlying vector field $v_\theta(x, t)$, rather than modelling transport directly. The conditional probability paths $p_t(x | x_1)$ are trained between samples $x_0 \sim p_0$ and data points $x_1 \sim p_1$, with the regression objective

$$\mathcal{L}_{CFM} = E_{t, x_1, x_0} \|v_\theta(x_t, t) - u_t(x_t | x_1)\|^2. \quad (1)$$

This in turn requires no simulation, no explicit density evaluation, and no Jacobian computation [37]. A critical finding of prior CFM works is that we do not need to explicitly compute the optimal transport flow field u^* to serve as the “ground truth” target for our regression. Instead, we recover an equivalent flow field by marginalising over random draws from p_0 and p_1 with a simple and tractable pairwise path.

Diffusion can be viewed as a special case of CFM under a Gaussian linear path [15]:

$$v(x_t | x_0) = \mathcal{N}(x_t | a_t x_0, s_t^2 I), \quad a_t = \sqrt{\bar{\alpha}_t}, \quad s_t^2 = 1 - \bar{\alpha}_t, \quad (2)$$

where s_t and a_t represent the single step, and cumulative noising weight respectively, at t . DDPMs are then trained with the denoising objective

$$\mathcal{L}_{DDPM} = \frac{1}{2} \|v_\theta(x_t, t) - x_0\|^2, \quad (3)$$

and reverse-time updates (e.g., DDIM) at inference. In CFM, we choose the linear-Gaussian conditional path

$$x_t = (1 - t)x_0 + tx_1, \quad x_0 \sim \mathcal{N}(0, I), \quad (4)$$

whose conditional target flow field is the constant interpolant

$$u_t(x_t | x_1) = x_1 - x_0. \quad (5)$$

The neural network $v_\theta(x, t)$ is then trained through the objective in Eqn. 1. Because the underlying pairwise paths are linear, they by definition represent the shortest possible paths between samples. The intuition behind CFM is that marginalising over a collection of shortest possible paths, gives a resulting flow field that is close to the ideal optimal transport mapping. These simple and compact ODE flow fields can then be traversed efficiently in a few Euler steps at inference times with

$$x_{t+\Delta} = x_t + \hat{u}_\theta(x_t, t) \Delta. \quad (6)$$

This contrasts the complex SDE fields induced by diffusion, which must be traversed via many DDPM steps.

3.1.1. Detection with CFM

Object detection can be parameterized as conditional set prediction. Given an image $I \in \mathbb{R}^{H \times W \times 3}$ and its feature map \mathbf{p} , we define a probability distribution $p(\mathcal{Y} | F)$ over finite, order-agnostic sets $\mathcal{Y} = \{(b_i, c_i)\}_{i=1}^M$ with $M \in \mathbb{N}_0$ varying per image. Each element comprises a bounding box $b_i = (c_x, c_y, w, h) \in \mathbb{R}^4$ and a class label $c_i \in \{1, \dots, K\}$, with (c_x, c_y) defining the center coordinates and (w, h) the width/height of the i -th bounding box within a particular set.

In this work, to apply the theoretical framework of CFM to the task of object detection, we treat x_1 as a ground truth set of bounding boxes \mathcal{Y} and x_0 as a set of proposals sampled from a simple prior distribution. Training a neural network through the regression objective in Eqn. 1 yields a flow field that transports samples from the prior to predicted endpoints \hat{x}_1 . To further align this formalization of CFM to the detection task, rather than predicting a velocity, we predict the endpoint \hat{x}_1 and class label \hat{c} while recovering the velocity algebraically for sampling during inference as

$$\hat{u}_t = \hat{x}_1 - x_0, \text{ where } \hat{x}_1 = v_\theta(x_t, t), \quad (7)$$

which enables standard detection-oriented set losses on \hat{x}_1, \hat{c} , tightly coupling the training objective to the task [6, 10, 29].

3.2. Architecture

To allow fair comparison to previous generative detectors like DiffusionDet, we adopt the Sparse R-CNN base architecture. As shown in Figure 2, the model can be viewed as two primary components, an image encoder and detection decoder along with a prior statistics predictor in the case of data-dependant priors.

3.2.1. Image Encoder

A standard vision backbone (ResNet [25] with a Feature Pyramid Network [35]) maps images $I \in \mathbb{R}^{C \times H \times W}$ to rich

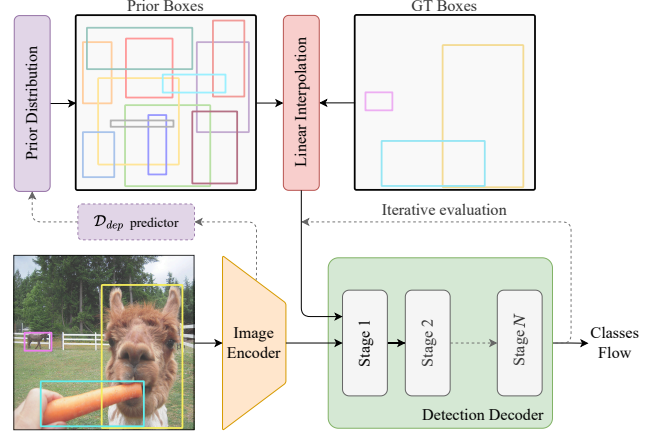


Figure 2. Architecture block diagram of FlowDet.

multi-scale feature maps

$$\{\mathbf{p}_\ell\}_{\ell \in \mathcal{L}} = \text{FPN}(\text{Backbone}(I)), \quad (8)$$

where ℓ indicates the featuremap at a particular pyramid level, and $\mathbf{p}_\ell \in \mathbb{R}^{D \times H_\ell \times W_\ell}$ are time-invariant and reused across all timesteps.

3.2.2. Prior Distribution

Unlike diffusion models, CFM allows for the exploration of alternate choices of prior distributions, including data-derived or data-dependent distributions. Theoretically, through closer alignment of the prior distribution to the ground truth distribution, the conditional paths between a sample point x_0 and data point x_1 are both shorter and straighter. These simplified paths improve the efficiency of the integration process, at the cost of reducing exploration and increasing redundancy between boxes.

In this section we will formulate a range of possible prior distributions, which will then be ablated in Section 4.3.1. Our base prior distribution is defined as $\mathcal{D}_{GaussN} = \mathcal{N}(0, 1)$ inline with diffusion. We define “data-derived” as a set of prior distributions that are pre-computed from the dataset statistics and applied uniformly over all incoming samples. Meanwhile we define “data-dependant” as distribution statistics that are learnt during training.

More specifically we implement the data-derived prior \mathcal{D}_{der} as a Gaussian whose mean and standard deviation match those aggregated across all the ground-truth bounding boxes in the dataset. We extend this idea with \mathcal{D}_{der-sb} as a Mixture of Gaussians, each of which is fit to a size-bucketed subset of the ground-truth bounding boxes. In contrast, a data-dependant prior \mathcal{D}_{dep} predicts the statistics per image

$$(\hat{\mu}, \hat{\sigma}) = \text{Sigmoid}(\text{MLP}(\text{GAP}(\mathbf{p}_{-1}))), \quad (9)$$

where GAP takes a Global Average Pool of the coarsest feature map \mathbf{p}_{-1} to generate a feature vector and MLP is

a simple two layer Multi Layer Perceptron. We outline the supervision of \mathcal{D}_{der-sb} during training in Section 3.3.3.

To ensure that RoIs derived from bounding boxes crop valid regions of images, the prior distributions are sampled via inverse Cumulative Distribution Function (CDF) sampling from a factorized truncated normal.

3.2.3. Detection Decoder

We use a DynamicHead architecture similar to Sparse R-CNN [58] which consists of six stages. Stage n of the head crops the feature maps from the image encoder, \mathbf{p}_ℓ , to obtain RoI features $\mathbf{r}_t^n = \text{RoIAlign}(\mathbf{p}_\ell, x_t^n)$. The RoI features are then processed into object features h_t^n through an RC-NNHead [58] with multi-head shared attention, dynamic instance interaction and a feedforward network,

$$h_t^n = \text{FFN}(\text{DynamicHead}(\text{MHSA}(\mathbf{r}_t^n, \tilde{h}_t^{n-1}))). \quad (10)$$

To produce \tilde{h}_t^n , we condition h_t^n with the current timestep t by first applying sinusoidal embedding [62] $\tau = \phi(t)$ then, following FiLM [47], we project the embedding to a scale γ and shift β such that

$$\tilde{h}_t^n = \gamma(\tau) \odot h_t^n + \beta(\tau). \quad (11)$$

The time-conditioned object features \tilde{h}_t^n are then jointly used to predict a bounding box offset ($\Delta\hat{x}$) and classification label (\hat{c}) from the CFM model

$$(\Delta\hat{x}_t^n, \hat{c}_t^n) = v_\theta^n(\tilde{h}_t^{n-1}). \quad (12)$$

The output offsets are then applied to the bounding box proposals before being iteratively fed to the next head stage

$$\hat{x}_t^n = \hat{x}_t^{n-1} + \Delta\hat{x}_t^n. \quad (13)$$

We train the model using a single randomly selected timestep per sample, to ensure broad coverage of the flow field. At inference time, we draw N_{eval} timesteps from a linear schedule ($[t_1, \dots, t_{N_{eval}}]$). The full head (including all stages) is then called in turn, with the output of the final head stage feeding in as input to the first head stage at the next time step. More formally, the initial conditions for Eqn. 13 at each timestep are $\hat{x}_{t_i}^0 = \hat{x}_{t_{i-1}}^N + \Delta\hat{x}_{t_{i-1}}^N$.

3.3. Training

During training, the model is fed with the interpolants u_t constructed according to the conditional paths defined in Equation 5. As such, we replace the traditional Region Proposal Network [49] or learnt bounding box proposals [58] with a random set of source boxes sampled from the chosen prior distribution. Each source sample, x_0 , from the prior distribution must be paired with a valid ground truth sample, x_1 as outlined below.

3.3.1. Ground Truth Padding

In practice, each image contains a varying number of ground truth boxes, N_{gt} . Since we must assign each source sample to a target box, we must pad the ground truth set to match the chosen number of training proposals, N_{train} . We follow DiffusionDet’s empirical findings and pad N_{gt} with random samples of the source distribution which proves more effective than crude duplications of the ground truth boxes.

3.3.2. Interpolant construction

In the same way that CFM supports a range of prior distributions, it is possible to employ a range of matching strategies between source and target samples. In its vanilla form, CFM employs random pairing of x_1 samples against x_0 samples. We call this matching strategy \mathcal{M}_{rand} . However, this can be slow to converge as many training pairs lie far from the optimal transport path. To accelerate convergence we can implement mini-batch OT [60] by employing Hungarian matching between source and target sets. We refer to this matching strategy as \mathcal{M}_{hung} . This can focus training budget on the pairs that are closer to the optimal transport paths, but it can leave less common areas of the flow field under-constrained. When employing hungarian matching, we explore a range of different similarity measures between boxes including: centrepoint distance (\mathcal{M}_{hung-c}) which is scale agnostic, generalised IoU (gIoU) [50] + bounding box difference (\mathcal{M}_{hung-g}) and InterpIoU (\mathcal{M}_{hung-i}) [38]. Both gIoU and InterpIoU are intended to measure overlap, but in a manner that decays smoothly for non-overlapping boxes.

Regardless of the matching strategy, the paired samples are then constructed into CFM interpolants as defined in Eqn. 4 with $t \sim U[0, 1]$ in contrast to the cosine schedule commonly adopted with diffusion.

3.3.3. Training supervision

While the Gaussian and data-derived prior distributions outlined in Sec. 3.2.2 are static and have no trainable parameters, the data-dependent prior is supervised in isolation to the detection decoder as sampling the truncated Gaussian distributions prevents gradient flow. Therefore, the predicted $\hat{\mu}, \hat{\sigma}$ are regressed against the mean and std. dev. of ground truth boxes within the batch.

The outputs from each stage in the detection decoder (\hat{x}_1, \hat{c}) are independently supervised against the ground truth set (x_1, c) through the standard set prediction loss popularised by [6]. The full definition of the training loss (including the one-to-many assignment of predictions to ground-truth) is provided in Appendix A. However, in summary, it comprises

$$\mathcal{L}_{match} = \lambda_{cls} \cdot \mathcal{L}_{cls} + \lambda_{\ell_1} \cdot \mathcal{L}_{\ell_1} + \lambda_{gIoU} \cdot \mathcal{L}_{gIoU}. \quad (14)$$

Here, we define \mathcal{L}_{cls} as focal loss between \hat{c} and c , \mathcal{L}_{ℓ_1} and \mathcal{L}_{gIoU} as the ℓ_1 and gIoU loss, respectively, between \hat{x} and x . λ_{cls} , λ_{ℓ_1} and λ_{gIoU} define their respective weights.

3.4. Inference

At inference, we sample an arbitrary sized set of N_{eval} boxes from the prior distribution and integrate them through the latent flow field within the detection decoder with an ODE solver. Given the strong single step performance of the detection decoder, we implement a simple Euler integrator and ablate higher order solvers in Sec. 4.3.2.

During integration with multiple sampling steps, weak predictions are discarded per step based on intermediate classification scores and the set of proposals is replenished with new samples from the prior distribution following [10]. Outputs across each sampling step are aggregated as an ensemble set of predictions with Non-Maximal Suppression (NMS) to reduce trivial duplicates between steps. The final set of bounding boxes post-filtering are resized and clipped such that the predictions are bounded to the image size.

4. Experiments

We benchmark FlowDet on both standard (COCO) and fine-grained (LVIS) detection tasks. We compare with common baseline detectors covering a range of performance intervals. We also provide detailed comparisons against DiffusionDet to highlight the stronger accuracy/compute trade-off within the scope of generative object detection. Following this, we explore and ablate design choices in Section 4.3.

Common Objects in COntext (COCO) [34] has been established as the de facto benchmark for object detection and other tasks (panoptic segmentation, keypoint detection, etc.). We follow the commonplace practice of using the 2017 train/val split that contains 118K/5k images respectively. Objects within images are classified into 80 categories with images including both sparse and crowded context-rich scenes. Evaluation is quantified with the Mean Average Precision (mAP, often denoted as AP) metric that reports AP averaged over IoU thresholds ranging from 0.5:0.95 and additional small/medium/large scale stratified AP measures.

The Large Vocabulary Instance Segmentation (LVIS) [23] dataset extends COCO’s annotations to a large-vocabulary, long-tail setting that further exemplifies the frequency imbalance of objects in real-world imagery. In this case we follow the standard protocol and report frequency stratified AP measures (AP_{rare} , AP_{common} , $AP_{frequent}$) that differentiate between performance on classes with a high number of instances.

4.1. Experimental Setup

We evaluate our technique using two backbone models: ResNet50 and ResNet101 with FPN, all initialised with pre-trained weights from ImageNet [12] pre-training as outlined in Detectron2’s model zoo [65]. All models are initialised with 6 head stages and are trained to a standard COCO 3x schedule, adjusted for a batch size of 8, resulting in approx. 532k iterations for a single GPU at a learning rate of

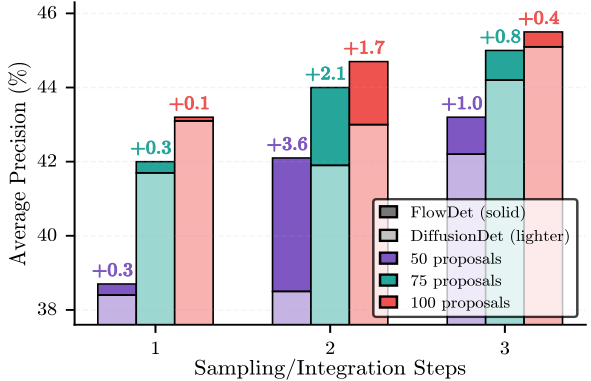


Figure 3. Plot of AP against integration steps between FlowDet and DiffusionDet. We plot AP for $N_{eval} \in \{50, 75, 100\}$.

2.5×10^{-5} with weight decay of 1×10^{-4} . The learning rate is linearly warmed up for 1000 iterations then scheduled to decay by a factor of $0.1 \times$ after $2/3$ and $8/9$ of the total training iterations. Following [6], we set the matching cost and loss weightings defined in Eqns. 14 to $\lambda_{cls} = 2.0$, $\lambda_{\ell_1} = 5.0$ and $\lambda_{gIoU} = 2.0$. Data augmentations during training consist of random horizontal flips, crops and scale jitter, that resizes images such that the shortest and longest edges are between 480-800 pixels and 1333 pixels respectively.

In terms of CFM specific setup, we chose to set our prior distribution to a standard Gaussian, with random pairing, and a simple Euler ODE integrator for inference. These settings are derived from our ablations conducted in each area, as described in Section 4.3.

At inference, we evaluate the model with various numbers of boxes and integration steps to highlight the flexibility of FlowDet without re-training, following [10]. To clearly demonstrate the capabilities of generative detectors, we constrain recall and isolate the effects of the generative transport mechanism from the effect of having many highly redundant proposals. We therefore evaluate with $N_{eval} \in \{50, 75, 100\}$ proposal boxes, while still training with $N_{train} = 300$ to accelerate convergence and ensure flow field coverage. The post processing pipeline includes default rescaling and clipping of predictions with class-wise NMS, with an IoU threshold of 0.6, to suppress duplicates introduced by the top-k matching in the set prediction losses.

4.2. Results

We first present our results on the validation split of COCO using 2 different feature backbones, in Table 1 alongside strong non-generative baselines and DiffusionDet as a generative comparison. FlowDet surpasses all the non-generative baselines across almost all metrics and backbones. For example, a margin of $+0.5\%$ AP over Sparse R-CNN with three integration steps. Similarly, FlowDet outperforms DiffusionDet across almost all metrics, at all operating points, with both feature backbones. In the single-step base case (where the flow field is weakly utilised) we achieve a slight

advantage of +0.1% AP.

When introducing a few iterative evaluation steps, FlowDet scales more rapidly than DiffusionDet, resulting in a +0.4% AP gain in the 3 step setting. These strengths in iterative evaluation are repeated with stronger backbones, validating the potential for FlowDet to scale with more expressive image encoders. Figure 3 shows that in a recall-constrained regime with only 50 proposals, FlowDet delivers a +3.6% AP gain over DiffusionDet at comparable compute, indicating more efficient usage of proposals with lower redundancy. When the proposal budget is low, the transport paths from initial boxes to targets are naturally longer, and the detection head has fewer opportunities to “shortcut” the transport via lucky source samples. This highlights how CFM’s more direct flows yield more reliable localization. As the number of proposals increases, both methods benefit from denser shortcuts, but FlowDet maintains a consistent advantage across steps and proposal counts.

Evaluating on LVIS with like-for-like settings as [10], FlowDet again shows strong scaling performance, outperforming other generative detection models across almost all metrics and operating points. Of particular note is FlowDet’s excellent performance on rare item categories, with improvements as high as 4.2% AP_{rare} in some cases.

4.2.1. Discussion

Overall we present strong evidence validating the improvements provided by CFM’s shorter, straighter transport paths, during generative detection. It is worth noting that we have focussed on providing a fair comparison against DiffusionDet, the only previous foray into generative detection. To enable this, we have adopted matching backbones and architectures which are no longer state-of-the-art. However, the concepts implemented in FlowDet are modular and can be adapted to work with any query set-based detector architecture. For example we have seen very promising preliminary results using advanced DINO based feature backbones and DETR style architectures. However, in this evaluation we focussed specifically on the differences between the stochastic SDE formulation of diffusion compared and the linear ODE formulation of CFM. While there are gains to be found through a greater number of diffusion steps, CFM transport or localisation of the boxes returns a higher level of performance per integration step. This observation aligns with the theory behind the two generative formulations. Under compute constrained settings, a more linear path results in less integration error compared to curved stochastic paths.

4.3. Ablation Study

This section details a number of ablations on the prior distribution selection, OT pairing strategy and ODE solver with runtime analysis. These are areas where CFM provides additional flexibility to FlowDet. To ease comparison, we fix the backbone to ResNet50, train to a 3x schedule and evaluate

Method	AP	AP ₅₀	AP ₇₅	AP _s	AP _m	AP _l
ResNet-50 [25]						
RetinaNet [65]	38.7	58.0	41.5	23.3	42.3	50.3
Faster R-CNN [65]	40.2	61.0	43.8	24.2	43.5	52.0
Cascade R-CNN [65]	44.3	62.2	48.0	26.6	47.7	57.7
DETR [6]	42.0	62.4	44.2	20.5	45.8	61.1
Deformable DETR [68]	43.8	62.6	47.7	26.4	47.1	58.0
Sparse R-CNN [58]	45.0	63.4	48.2	26.9	47.2	59.5
DiffusionDet [†] (100@1)	43.1	60.6	46.4	23.9	46.3	60.1
DiffusionDet [†] (100@2)	43.0	60.4	46.6	23.9	46.1	60.1
DiffusionDet [†] (100@3)	45.1	63.8	48.3	27.1	48.2	60.7
FlowDet (100@1)	43.2	60.9	46.7	24.9	46.4	60.0
FlowDet (100@2)	44.7	63.2	48.2	26.6	47.5	60.8
FlowDet (100@3)	45.5	64.1	49.2	27.9	48.4	61.5
ResNet-101 [25]						
RetinaNet [65]	40.4	60.2	43.2	24.0	44.3	52.2
Faster R-CNN [65]	42.0	62.5	45.9	25.2	45.6	54.6
Cascade R-CNN [7]	45.5	63.7	49.9	27.6	49.2	59.1
DETR [6]	43.5	63.8	46.4	21.9	48.0	61.8
Sparse R-CNN [58]	46.4	64.6	49.5	28.3	48.3	61.6
DiffusionDet [†] (100@1)	44.6	62.3	48.4	25.6	48.5	61.7
DiffusionDet [†] (100@2)	44.4	62.1	48.3	24.8	48.1	61.9
DiffusionDet [†] (100@3)	46.1	64.8	49.8	27.7	49.9	62.4
FlowDet (100@1)	44.0	62.1	47.5	25.7	47.4	61.1
FlowDet (100@2)	45.7	64.3	49.4	28.5	48.9	62.2
FlowDet (100@3)	46.1	65.1	50.0	28.7	49.5	62.6

Table 1. Comparison of object detector performance on the COCO 2017 validation set. Highlighting indicates the **best**, **second best** and **third best** result per metric. [$N_{eval}@S$] denotes the number of prior samples (N_{eval}) and number of iteration steps (S). [†]We re-train DiffusionDet with the standard 3x schedule inline with other non-DETR models.

Method	AP	AP ₅₀	AP ₇₅	AP _r	AP _c	AP _f
ResNet-50 [25]						
DiffusionDet [†] (100@1)	24.3	33.0	25.6	17.7	23.1	28.5
DiffusionDet [†] (100@2)	23.7	32.6	24.8	16.1	22.5	28.3
DiffusionDet [†] (100@3)	28.4	38.9	29.7	20.8	27.0	33.2
FlowDet (100@1)	23.4	32.3	24.5	16.6	22.1	27.9
FlowDet (100@2)	27.0	37.3	28.2	20.3	25.1	32.2
FlowDet (100@3)	28.7	39.7	30.2	22.0	26.7	33.9

Table 2. Comparison of object detector performance on the LVIS v1.0 validation set.

with 100 boxes at 1 to 3 integration steps. Additionally, the CFM settings are set to a default of a normal Gaussian prior distribution, random pairing of prior to ground truth samples and Euler ODE integration when not actively ablated.

4.3.1. Prior Distribution

Table 3 quantifies the effect of various prior distributions from which the x_0 set of proposal boxes are sampled. We test a normal Gaussian distribution (\mathcal{D}_{GaussN}), data-derived Gaussian parameters (global \mathcal{D}_{der} and size-bucketed \mathcal{D}_{der-sb}) and data-dependant Gaussian parameters (\mathcal{D}_{dep}) with the implementations defined in Section 3.2.2.

In this detection setting, a normal Gaussian performs

Prior Distribution	AP	AP ₅₀	AP ₇₅
100 boxes, 1 step			
Gaussian (\mathcal{D}_{GaussN})	43.2	60.9	46.7
Data-Driven (\mathcal{D}_{der})	42.4	59.8	45.8
Data-Driven size-bucketed (\mathcal{D}_{der-sb})	42.4	59.9	45.4
Data-Dependant (\mathcal{D}_{dep})	42.6	60.2	45.9
100 boxes, 2 steps			
Gaussian (\mathcal{D}_{GaussN})	44.7	63.2	48.2
Data-Driven (\mathcal{D}_{der})	44.6	63.4	48.2
Data-Driven size-bucketed (\mathcal{D}_{der-sb})	44.7	64.4	49.0
Data-Dependant (\mathcal{D}_{dep})	44.7	63.3	48.2
100 boxes, 3 steps			
Gaussian (\mathcal{D}_{GaussN})	45.5	64.1	49.2
Data-Driven (\mathcal{D}_{der})	45.0	63.4	48.2
Data-Driven size-bucketed (\mathcal{D}_{der-sb})	45.4	64.4	49.0
Data-Dependant (\mathcal{D}_{dep})	45.2	64.0	48.8

Table 3. Prior Distribution selection.

Cost function	AP	AP ₅₀	AP ₇₅
100 boxes, 1 step			
Random pairing (\mathcal{M}_{rand})	43.2	60.9	46.7
L2 cdist (\mathcal{M}_{hung-c})	42.9	60.7	46.2
ℓ_1 + gIoU (\mathcal{M}_{hung-g})	42.6	60.1	46.0
InterIoU (\mathcal{M}_{hung-i})	42.9	60.6	46.4
100 boxes, 2 step			
Random pairing (\mathcal{M}_{rand})	44.7	63.2	48.2
L2 cdist (\mathcal{M}_{hung-c})	44.3	62.7	47.6
ℓ_1 + gIoU (\mathcal{M}_{hung-g})	44.0	62.4	47.6
InterIoU (\mathcal{M}_{hung-i})	44.4	63.0	47.9
100 boxes, 3 step			
Random pairing (\mathcal{M}_{rand})	45.5	64.1	49.2
L2 cdist (\mathcal{M}_{hung-c})	44.8	63.5	48.5
ℓ_1 + gIoU (\mathcal{M}_{hung-g})	44.5	63.1	48.3
InterIoU (\mathcal{M}_{hung-i})	45.0	63.9	48.6

Table 4. OT Pairing Cost Functions.

the best as a prior distribution. We hypothesise that this is because more compact source distributions increase redundancy between the predicted boxes. In the single-step setting, the resulting loosely packed detection clusters interact poorly with NMS post-processing. However, it is noteworthy that as the number of inference steps increases, these duplicate sets tighten, making it easier for NMS to remove duplicates. This closes the gap between the Gaussian prior and data-derived/dependent priors at higher step counts.

4.3.2. Optimal Transport Pairing

In this ablation, we compare the source-to-target matching strategies described in Section 3.3.2. These include random pairing (\mathcal{M}_{rand}) against hungarian matching with three cost functions in Table 4: bounding box centre distance (\mathcal{M}_{hung-c}), bounding box distance + generalised IoU (\mathcal{M}_{hung-g}) and InterIoU (\mathcal{M}_{hung-i}). Interestingly, the results show that any form of coupling, whether primitive or task-aligned, results in worse overall detector performance. This is likely due to the classification head being starved of easy negative examples as most interpolants fed into the

ODE Solver	AP	AP ₅₀	AP ₇₅	FPS
100 boxes, 1 step				
DiffusionDet (DDIM)	43.1	60.6	46.4	73.5
Euler	43.2	60.9	46.7	73.5
Heun	28.6	40.9	30.2	50.0
RK4	1.2	4.3	0.4	31.1
100 boxes, 2 steps				
DiffusionDet (DDIM)	43.0	60.4	46.6	49.0
Euler	44.7	63.2	48.2	49.5
Heun	41.8	59.0	44.9	30.3
RK4	1.4	5.4	0.2	17.5
100 boxes, 3 steps				
DiffusionDet (DDIM)	45.1	63.8	48.3	37.0
Euler	45.5	64.1	49.2	37.3
Heun	44.2	62.3	47.7	21.9
RK4	1.7	6.1	0.4	12.3
100 boxes, adaptive steps				
DOPRI5 1-8 steps, atol=5	1.7	6.6	0.4	2.8
DOPRI5 1-16 steps, atol=3	1.5	5.7	0.3	1.4

Table 5. ODE Solver Methods. Note: FPS was computed using a single NVIDIA RTX 5090 for inference.

head are strongly aligned to a ground truth target. In turn, at inference time, boxes with a high classification scores that do not overlap a targets are significantly penalised.

Of the remaining matchers, InterIoU performs the best, with the arrangement of the matchers remaining roughly stable regardless of the number of inference steps.

4.3.3. ODE Solver and Runtime Analysis

Finally, we compare ODE solvers across accuracy and runtime in Table 4.3.3. Euler consistently matches or exceeds the speed of DDIM while achieving greater performance (e.g., 45.5 vs. 45.1 AP at ≈ 37 FPS, 3 steps). In contrast, higher-order solvers suffer at coarser schedules: Heun recovers only by 3 steps and is slower, RK4 [3] is numerically brittle with near-zero AP, and the adaptive DOPRI5 [13] variant fails to reach a good solution within the step/tolerance caps and inference speed is drastically reduced.

5. Conclusion

This paper presents FlowDet, a generalisation of previous diffusion based object detectors to a broader category of modern generative models. Framing detection as a generative transport task brings numerous benefits including arbitrarily varying the precision, recall and computational cost of the predictions at run-time without model retraining.

By adopting a general Conditional Flow Matching formulation, we explore a broad range of source distributions, matching regimes and ODE solvers. Our results indicate that FlowDet outperforms DiffusionDet (and other non-generative detection baselines) across a broad range of operating points, feature backbones and datasets. These broad analyses will provide a solid foundation for future works in the generative detection field.

References

- [1] Michael Samuel Albergo and Eric Vanden-Eijnden. Building normalizing flows with stochastic interpolants. In *The Eleventh International Conference on Learning Representations*, 2023. 3
- [2] Michael S. Albergo, Nicholas M. Boffi, and Eric Vanden-Eijnden. Stochastic interpolants: A unifying framework for flows and diffusions, 2023. 3
- [3] J. C. Butcher. A history of runge-kutta methods. *Appl. Numer. Math.*, 20(3):247–260, 1996. 8
- [4] Zhi Cai, Songtao Liu, Guodong Wang, Zeming Li, Zheng Ge, Xiangyu Zhang, and Di Huang. Align-detr: Enhancing end-to-end object detection with aligned loss. In *35th British Machine Vision Conference 2024, BMVC 2024, Glasgow, UK, November 25-28, 2024*. BMVA, 2024. 2
- [5] Sergio Calvo-Ordóñez, Matthieu Meunier, Alvaro Carrea, Christoph Reisinger, Yarin Gal, and Jose Miguel Hernandez-Lobato. Weighted conditional flow matching, 2025. 3
- [6] Nicolas Carion, Francisco Massa, Gabriel Synnaeve, Nicolas Usunier, Alexander Kirillov, and Sergey Zagoruyko. End-to-end object detection with transformers. In *European Conference on Computer Vision (ECCV)*, 2020. 1, 2, 4, 5, 6, 7
- [7] Kai Chen, Jiaqi Wang, Jiangmiao Pang, Yuhang Cao, Yu Xiong, Xiaoxiao Li, Shuyang Sun, Wansen Feng, Ziwei Liu, Jiarui Xu, Zheng Zhang, Dazhi Cheng, Chenchen Zhu, Tianheng Cheng, Qijie Zhao, Buyu Li, Xin Lu, Rui Zhu, Yue Wu, Jifeng Dai, Jingdong Wang, Jianping Shi, Wanli Ouyang, Chen Change Loy, and Dahua Lin. MMDetection: Open mmlab detection toolbox and benchmark. *arXiv preprint arXiv:1906.07155*, 2019. 7
- [8] Qiang Chen, Xiaokang Chen, Jian Wang, Shan Zhang, Kun Yao, Haocheng Feng, Junyu Han, Errui Ding, Gang Zeng, and Jingdong Wang. Group detr: Fast detr training with groupwise one-to-many assignment. In *Proceedings of the IEEE International Conference on Computer Vision (ICCV)*, 2023. 2
- [9] Ricky T. Q. Chen, Yulia Rubanova, Jesse Bettencourt, and David K Duvenaud. Neural ordinary differential equations. In *Advances in Neural Information Processing Systems*. Curran Associates, Inc., 2018. 3
- [10] Shoufa Chen, Peize Sun, Yibing Song, and Ping Luo. Diffusiondet: Diffusion model for object detection. In *Proceedings of the IEEE/CVF International Conference on Computer Vision (ICCV)*, pages 19830–19843, 2023. 1, 2, 4, 6, 7
- [11] Xiyang Dai, Yinpeng Chen, Jianwei Yang, Pengchuan Zhang, Lu Yuan, and Lei Zhang. Dynamic detr: End-to-end object detection with dynamic attention. In *Proceedings of the IEEE/CVF International Conference on Computer Vision (ICCV)*, pages 2988–2997, 2021. 2
- [12] Jia Deng, Wei Dong, Richard Socher, Li-Jia Li, Kai Li, and Li Fei-Fei. Imagenet: A large-scale hierarchical image database. In *2009 IEEE Conference on Computer Vision and Pattern Recognition*, pages 248–255, 2009. 6
- [13] J.R. Dormand and P.J. Prince. A family of embedded runge-kutta formulae. *Journal of Computational and Applied Mathematics*, 6(1):19–26, 1980. 8
- [14] Kaiwen Duan, Song Bai, Lingxi Xie, Honggang Qi, Qingming Huang, and Qi Tian. Centernet: Keypoint triplets for object detection. In *Proceedings of the IEEE/CVF International Conference on Computer Vision (ICCV)*, 2019. 2
- [15] Ruiqi Gao, Emiel Hoogeboom, Jonathan Heek, Valentin De Bortoli, Kevin P. Murphy, and Tim Salimans. Diffusion meets flow matching: Two sides of the same coin. 2024. 3
- [16] Zheng Ge, Songtao Liu, Zeming Li, Osamu Yoshie, and Jian Sun. Ota: Optimal transport assignment for object detection. In *2021 IEEE/CVF Conference on Computer Vision and Pattern Recognition (CVPR)*, pages 303–312, 2021. 1
- [17] Zheng Ge, Songtao Liu, Feng Wang, Zeming Li, and Jian Sun. Yolox: Exceeding yolo series in 2021, 2021. 1
- [18] Adam P. Generale, Andreas E. Robertson, and Surya R. Kalidindi. Conditional variable flow matching: Transforming conditional densities with amortized conditional optimal transport, 2025. 3
- [19] Ross Girshick. Fast r-cnn. In *2015 IEEE International Conference on Computer Vision (ICCV)*, pages 1440–1448, 2015. 1, 2
- [20] Ross Girshick, Jeff Donahue, Trevor Darrell, and Jitendra Malik. Rich feature hierarchies for accurate object detection and semantic segmentation. In *Proceedings of the IEEE Conference on Computer Vision and Pattern Recognition (CVPR)*, 2014. 2
- [21] Will Grathwohl, Ricky T. Q. Chen, Jesse Bettencourt, and David Duvenaud. Scalable reversible generative models with free-form continuous dynamics. In *International Conference on Learning Representations*, 2019. 3
- [22] Pengsheng Guo and Alex Schwing. Variational rectified flow matching, 2025. 3
- [23] Agrim Gupta, Piotr Dollar, and Ross Girshick. LVIS: A dataset for large vocabulary instance segmentation. In *Proceedings of the IEEE Conference on Computer Vision and Pattern Recognition*, 2019. 6
- [24] Yizeng Han, Gao Huang, Shiji Song, Le Yang, Honghui Wang, and Yulin Wang. Dynamic neural networks: A survey. *IEEE Transactions on Pattern Analysis and Machine Intelligence*, 44:7436–7456, 2021. 1
- [25] Kaiming He, Xiangyu Zhang, Shaoqing Ren, and Jian Sun. Deep residual learning for image recognition. In *Proceedings of the IEEE Conference on Computer Vision and Pattern Recognition (CVPR)*, 2016. 2, 4, 7, 1
- [26] Jonathan Ho, Ajay Jain, and Pieter Abbeel. Denoising diffusion probabilistic models. In *Advances in Neural Information Processing Systems*, pages 6840–6851. Curran Associates, Inc., 2020. 2, 3
- [27] Qinghang Hong, Fengming Liu, Dong Li, Ji Liu, Lu Tian, and Yi Shan. Dynamic sparse r-cnn. In *2022 IEEE/CVF Conference on Computer Vision and Pattern Recognition (CVPR)*, pages 4713–4722, 2022. 2
- [28] Zemin Huang, Zhengyang Geng, Weijian Luo, and Guo-Jun Qi. One-step flow matching generators, 2025. 3
- [29] Ding Jia, Yuhui Yuan, Haodi He, Xiaopei Wu, Haojun Yu, Weihong Lin, Lei Sun, Chao Zhang, and Han Hu. Detsr with hybrid matching. In *2023 IEEE/CVF Conference on Computer Vision and Pattern Recognition (CVPR)*, pages 19702–19712, 2023. 4

- [30] Tero Karras, Miika Aittala, Timo Aila, and Samuli Laine. Elucidating the design space of diffusion-based generative models. In *Advances in Neural Information Processing Systems*, pages 26565–26577. Curran Associates, Inc., 2022. 3
- [31] Min Je Kim, Muhammad Munsif, Altaf Hussain, Hikmat Yar, and Sung Wook Baik. Pseudo-labeling driven refinement of benchmark object detection datasets via analysis of learning patterns, 2025. 3
- [32] Feng Li, Hao Zhang, Shilong Liu, Jian Guo, Lionel M Ni, and Lei Zhang. Dn-detr: Accelerate detr training by introducing query denoising. In *Proceedings of the IEEE/CVF Conference on Computer Vision and Pattern Recognition*, pages 13619–13627, 2022. 2
- [33] Yanghao Li, Hanzi Mao, Ross Girshick, and Kaiming He. Exploring plain vision transformer backbones for object detection. In *Computer Vision – ECCV 2022*, pages 280–296, Cham, 2022. Springer Nature Switzerland. 1
- [34] Tsung-Yi Lin, Michael Maire, Serge Belongie, James Hays, Pietro Perona, Deva Ramanan, Piotr Dollár, and C. Lawrence Zitnick. Microsoft coco: Common objects in context. In *Computer Vision – ECCV 2014*, pages 740–755, Cham, 2014. Springer International Publishing. 2, 6
- [35] Tsung-Yi Lin, Piotr Dollár, Ross Girshick, Kaiming He, Bharath Hariharan, and Serge Belongie. Feature pyramid networks for object detection. In *2017 IEEE Conference on Computer Vision and Pattern Recognition (CVPR)*, pages 936–944, 2017. 4
- [36] Tsung-Yi Lin, Priya Goyal, Ross Girshick, Kaiming He, and Piotr Dollar. Focal loss for dense object detection. In *Proceedings of the IEEE International Conference on Computer Vision (ICCV)*, 2017. 2, 1
- [37] Yaron Lipman, Ricky T. Q. Chen, Heli Ben-Hamu, Maximilian Nickel, and Matthew Le. Flow matching for generative modeling. In *The Eleventh International Conference on Learning Representations*, 2023. 2, 3
- [38] Haoyuan Liu and Hiroshi Watanabe. Interpiou: Rethinking bounding box regression with interpolation-based iou optimization, 2025. 5
- [39] Shilong Liu, Feng Li, Hao Zhang, Xiao Yang, Xianbiao Qi, Hang Su, Jun Zhu, and Lei Zhang. DAB-DETR: Dynamic anchor boxes are better queries for DETR. In *International Conference on Learning Representations*, 2022. 2
- [40] Wei Liu, Dragomir Anguelov, Dumitru Erhan, Christian Szegedy, Scott Reed, Cheng-Yang Fu, and Alexander C. Berg. Ssd: Single shot multibox detector. In *Computer Vision – ECCV 2016*, pages 21–37, Cham, 2016. Springer International Publishing. 2
- [41] Xingchao Liu, Chengyue Gong, and qiang liu. Flow straight and fast: Learning to generate and transfer data with rectified flow. In *The Eleventh International Conference on Learning Representations*, 2023. 3
- [42] Cheng Lu, Yuhao Zhou, Fan Bao, Jianfei Chen, Chongxuan LI, and Jun Zhu. Dpm-solver: A fast ode solver for diffusion probabilistic model sampling in around 10 steps. In *Advances in Neural Information Processing Systems*, pages 5775–5787. Curran Associates, Inc., 2022. 1
- [43] Cheng Lu, Yuhao Zhou, Fan Bao, Jianfei Chen, Chongxuan Li, and Jun Zhu. Dpm-solver++: Fast solver for guided sampling of diffusion probabilistic models. *Machine Intelligence Research*, 22(4):730–751, 2025. 1
- [44] Depu Meng, Xiaokang Chen, Zejia Fan, Gang Zeng, Houqiang Li, Yuhui Yuan, Lei Sun, and Jingdong Wang. Conditional detr for fast training convergence. In *Proceedings of the IEEE/CVF International Conference on Computer Vision (ICCV)*, pages 3651–3660, 2021. 2
- [45] Alexander Quinn Nichol and Prafulla Dhariwal. Improved denoising diffusion probabilistic models. In *Proceedings of the 38th International Conference on Machine Learning*, pages 8162–8171. PMLR, 2021. 3
- [46] George Papamakarios, Eric Nalisnick, Danilo Jimenez Rezende, Shakir Mohamed, and Balaji Lakshminarayanan. Normalizing flows for probabilistic modeling and inference. *Journal of Machine Learning Research*, 22(57):1–64, 2021. 3
- [47] Ethan Perez, Florian Strub, Harm de Vries, Vincent Dumoulin, and Aaron Courville. Film: visual reasoning with a general conditioning layer. In *Proceedings of the Thirty-Second AAAI Conference on Artificial Intelligence and Thirtieth Innovative Applications of Artificial Intelligence Conference and Eighth AAAI Symposium on Educational Advances in Artificial Intelligence*. AAAI Press, 2018. 5
- [48] Joseph Redmon, Santosh Divvala, Ross Girshick, and Ali Farhadi. You only look once: Unified, real-time object detection. In *Proceedings of the IEEE Conference on Computer Vision and Pattern Recognition (CVPR)*, 2016. 2
- [49] Shaoqing Ren, Kaiming He, Ross Girshick, and Jian Sun. Faster r-cnn: Towards real-time object detection with region proposal networks. *IEEE Transactions on Pattern Analysis and Machine Intelligence*, 39(6):1137–1149, 2017. 1, 2, 5
- [50] Hamid Rezatofighi, Nathan Tsoi, JunYoung Gwak, Amir Sadeghian, Ian Reid, and Silvio Savarese. Generalized intersection over union: A metric and a loss for bounding box regression. In *2019 IEEE/CVF Conference on Computer Vision and Pattern Recognition (CVPR)*, pages 658–666, 2019. 5, 1
- [51] Byungseok Roh, JaeWoong Shin, Wuhyun Shin, and Sae-hoon Kim. Sparse DETR: Efficient end-to-end object detection with learnable sparsity. In *International Conference on Learning Representations*, 2022. 2
- [52] Tim Salimans and Jonathan Ho. Progressive distillation for fast sampling of diffusion models. In *International Conference on Learning Representations*, 2022. 1
- [53] Oriane Siméoni, Huy V. Vo, Maximilian Seitzer, Federico Baldassarre, Maxime Oquab, Cijo Jose, Vasil Khalidov, Marc Szafraniec, Seungeun Yi, Michaël Ramamonjisoa, Francisco Massa, Daniel Haziza, Luca Wehrstedt, Jianyuan Wang, Timothée Darcet, Théo Moutakanni, Leonel Sentana, Claire Roberts, Andrea Vedaldi, Jamie Tolan, John Brandt, Camille Couprie, Julien Mairal, Hervé Jégou, Patrick Labatut, and Piotr Bojanowski. DINOv3, 2025. 1
- [54] Charlie Snell, Jaehoon Lee, Kelvin Xu, and Aviral Kumar. Scaling llm test-time compute optimally can be more effective than scaling model parameters, 2024. 1

- [55] Jascha Sohl-Dickstein, Eric Weiss, Niru Maheswaranathan, and Surya Ganguli. Deep unsupervised learning using nonequilibrium thermodynamics. In *Proceedings of the 32nd International Conference on Machine Learning*, pages 2256–2265, Lille, France, 2015. PMLR. 3
- [56] Jiaming Song, Chenlin Meng, and Stefano Ermon. Denoising diffusion implicit models. In *International Conference on Learning Representations*, 2021. 2, 3
- [57] Yang Song, Prafulla Dhariwal, Mark Chen, and Ilya Sutskever. Consistency models. In *Proceedings of the 40th International Conference on Machine Learning*, pages 32211–32252. PMLR, 2023. 1
- [58] Peize Sun, Rufeng Zhang, Yi Jiang, Tao Kong, Chenfeng Xu, Wei Zhan, Masayoshi Tomizuka, Lei Li, Zehuan Yuan, Changhu Wang, and Ping Luo. Sparse r-cnn: End-to-end object detection with learnable proposals. In *Proceedings of the IEEE/CVF Conference on Computer Vision and Pattern Recognition (CVPR)*, pages 14454–14463, 2021. 1, 2, 5, 7
- [59] Zhi Tian, Chunhua Shen, Hao Chen, and Tong He. Fcos: Fully convolutional one-stage object detection. In *Proceedings of the IEEE/CVF International Conference on Computer Vision (ICCV)*, 2019. 2
- [60] Alexander Tong, Kilian FATRAS, Nikolay Malkin, Guillaume Hugué, Yanlei Zhang, Jarrid Rector-Brooks, Guy Wolf, and Yoshua Bengio. Improving and generalizing flow-based generative models with minibatch optimal transport. *Transactions on Machine Learning Research*, 2024. Expert Certification. 3, 5
- [61] J. R. R. Uijlings, K. E. A. van de Sande, T. Gevers, and A. W. M. Smeulders. Selective search for object recognition. *International Journal of Computer Vision*, 104(2):154–171, 2013. 2
- [62] Ashish Vaswani, Noam Shazeer, Niki Parmar, Jakob Uszkoreit, Llion Jones, Aidan N Gomez, Łukasz Kaiser, and Illia Polosukhin. Attention is all you need. In *Advances in Neural Information Processing Systems*. Curran Associates, Inc., 2017. 2, 5
- [63] Xuezhi Wang, Jason Wei, Dale Schuurmans, Quoc Le, Ed H. Chi, Sharan Narang, Aakanksha Chowdhery, and Denny Zhou. Self-consistency improves chain of thought reasoning in language models. In *International Conference on Learning Representations (ICLR)*, 2023. 1
- [64] Yingming Wang, Xiangyu Zhang, Tong Yang, and Jian Sun. Anchor detr: Query design for transformer-based detector. In *Proceedings of the AAAI Conference on Artificial Intelligence*, pages 2567–2575, 2022. 2
- [65] Yuxin Wu, Alexander Kirillov, Francisco Massa, Wan-Yen Lo, and Ross Girshick. Detectron2. <https://github.com/facebookresearch/detectron2>, 2019. 6, 7
- [66] Tianyu Xie, Yu Zhu, Longlin Yu, Tong Yang, Ziheng Cheng, Shiyue Zhang, Xiangyu Zhang, and Cheng Zhang. Reflected flow matching. In *Proceedings of the 41st International Conference on Machine Learning*, pages 54614–54634. PMLR, 2024. 3
- [67] Zhuyu Yao, Jiangbo Ai, Boxun Li, and Chi Zhang. Efficient detr: Improving end-to-end object detector with dense prior, 2021. 2
- [68] Xizhou Zhu, Weijie Su, Lewei Lu, Bin Li, Xiaogang Wang, and Jifeng Dai. Deformable {detr}: Deformable transformers for end-to-end object detection. In *International Conference on Learning Representations*, 2021. 2, 7
- [69] Zhuofan Zong, Guanglu Song, and Yu Liu. Dets with collaborative hybrid assignments training. In *Proceedings of the IEEE/CVF international conference on computer vision*, pages 6748–6758, 2023. 2

A. Formulation of Training Loss

We provide a more detailed description of the training supervision, covered in Section 3.3.3 as follows.

A.1. \mathcal{D}_{dep} Prior Distribution Supervision

Given a set of predictions for the data-dependent prior distribution statistics $(\hat{\mu}, \hat{\sigma})$ as defined in Eqn. 9, we define the simple Mean-Squared-Error (MSE) loss as

$$\mathcal{L}_{prior} = \|\hat{\mu} - \mu\|_2^2 + \|\hat{\sigma} - \sigma\|_2^2, \quad (15)$$

where (μ, σ) are the mean and standard deviation of the ground-truth bounding boxes computed per batch item.

A.2. Detection Decoder Supervision

The outputs from each stage in the detection decoder (\hat{x}_1, \hat{c}) are independently supervised against the ground truth set (x_1, c) through the standard set prediction loss popularised by [6]. Traditionally, bipartite matching (via the Hungarian algorithm) between the prediction and ground-truth sets yields a permutation that minimises a matching cost

$$\mathcal{C}_{match} = \lambda_{cls} \cdot \mathcal{C}_{cls} + \lambda_{\ell_1} \cdot \mathcal{C}_{\ell_1} + \lambda_{gIoU} \cdot \mathcal{C}_{gIoU}. \quad (16)$$

Here, we define \mathcal{C}_{cls} as focal loss [36] between \hat{c} and c , and \mathcal{C}_{ℓ_1} and \mathcal{C}_{gIoU} as the ℓ_1 and gIoU [50] box costs between \hat{x}_1 and x_1 , respectively. Additionally, λ_{cls} , λ_{ℓ_1} and λ_{gIoU} control the relative weighting of each component.

In our setting there are many more predictions than true objects, so a strict one-to-one permutation would discard useful supervision signal. Following [10, 16, 17], we replace the Hungarian matching with a one-to-many assignment that selects, for each ground-truth box, the top- k predictions with the lowest cost \mathcal{C}_{match} as positives. The resulting positive set is used to define the detection loss

$$\mathcal{L}_{match} = \lambda_{cls} \cdot \mathcal{L}_{cls} + \lambda_{\ell_1} \cdot \mathcal{L}_{\ell_1} + \lambda_{gIoU} \cdot \mathcal{L}_{gIoU}, \quad (17)$$

with \mathcal{L}_{cls} , \mathcal{L}_{ℓ_1} and \mathcal{L}_{gIoU} mirroring the components of \mathcal{C}_{match} as in Eqn. 16 but now used as loss terms with the same weights λ_{cls} , λ_{ℓ_1} and λ_{gIoU} . Predictions that are not selected for any ground-truth object are ignored in \mathcal{L}_{match} . We recompute this top- k assignment independently for every decoder stage and normalise the resulting loss for each stage by the number of positive matches.

B. DINOv3 ViT Backbones

To assess FlowDet with stronger foundation encoders, we further evaluate it with the DINOv3 ViT-16 backbone [53] in the base (B) variant. Here, the backbone is kept frozen and we attach a lightweight simple feature pyramid neck following ViTDet [33]. In contrast to a standard FPN, this neck constructs a multi-scale hierarchy directly from the

Backbone	Steps	AP	AP ₅₀	AP ₇₅	AP _s	AP _m	AP _l
ResNet-50 [25]	1	43.2	60.9	46.7	24.9	46.4	60.0
	2	44.7	63.2	48.2	26.6	47.5	60.8
	3	45.5	64.1	49.2	27.9	48.4	61.5
ResNet-101 [25]	1	44.0	62.1	47.5	25.7	47.4	61.1
	2	45.7	64.3	49.4	28.5	48.9	62.2
	3	46.1	65.1	50.0	28.7	49.5	62.6
DINOv3 ViT-16 Base [53]	1	45.2	66.1	49.1	24.1	50.1	66.1
	2	47.1	68.8	51.3	26.2	51.6	67.4
	3	47.6	69.8	51.6	27.2	52.2	67.3

Table 6. COCO 2017 validation performance of FlowDet with different backbones and integration steps. Highlighting indicates the **best**, **second best** and **third best** result per metric. All results are obtained with $N_{eval} = 100$ with the ‘‘Steps’’ column reporting the number of integration steps S used at inference.

final stride-16 ViT feature map using parallel convolutions and deconvolutions, without top-down or lateral connections between backbone stages. This design exploits the strong, single-scale representations learned by DINOv3 while injecting only minimal detection-specific structure. This allows our analysis to focus on the contributions of the FlowDet decoder when scaling to more powerful backbones, without confounding the findings with simultaneous innovations in the backbone architecture itself. We summarise the detection performance of the DINOv3-based backbone configuration in Table 6.

Across all settings, using a frozen DINOv3 ViT-16 backbone leads to consistent improvements over both ResNet baselines (Table 1) in these recall-constrained regimes. Impressively, this is achieved without increasing the compute budgets allocated for training or inference. In particular, the DINOv3-B configuration achieves 47.6% AP on COCO, compared to 45.5% AP with ResNet-50 or 46.1% AP with ResNet-101. Additionally, the gains are most pronounced at the AP₅₀ threshold with a +5.7% and +4.7% gain over ResNet-50 and ResNet-101 respectively. These results demonstrate that FlowDet scales favourably with modern backbones such as DINOv3 without any backbone fine-tuning, and that a simple feature pyramid remains sufficient when moving from convolutional to ViT encoders.

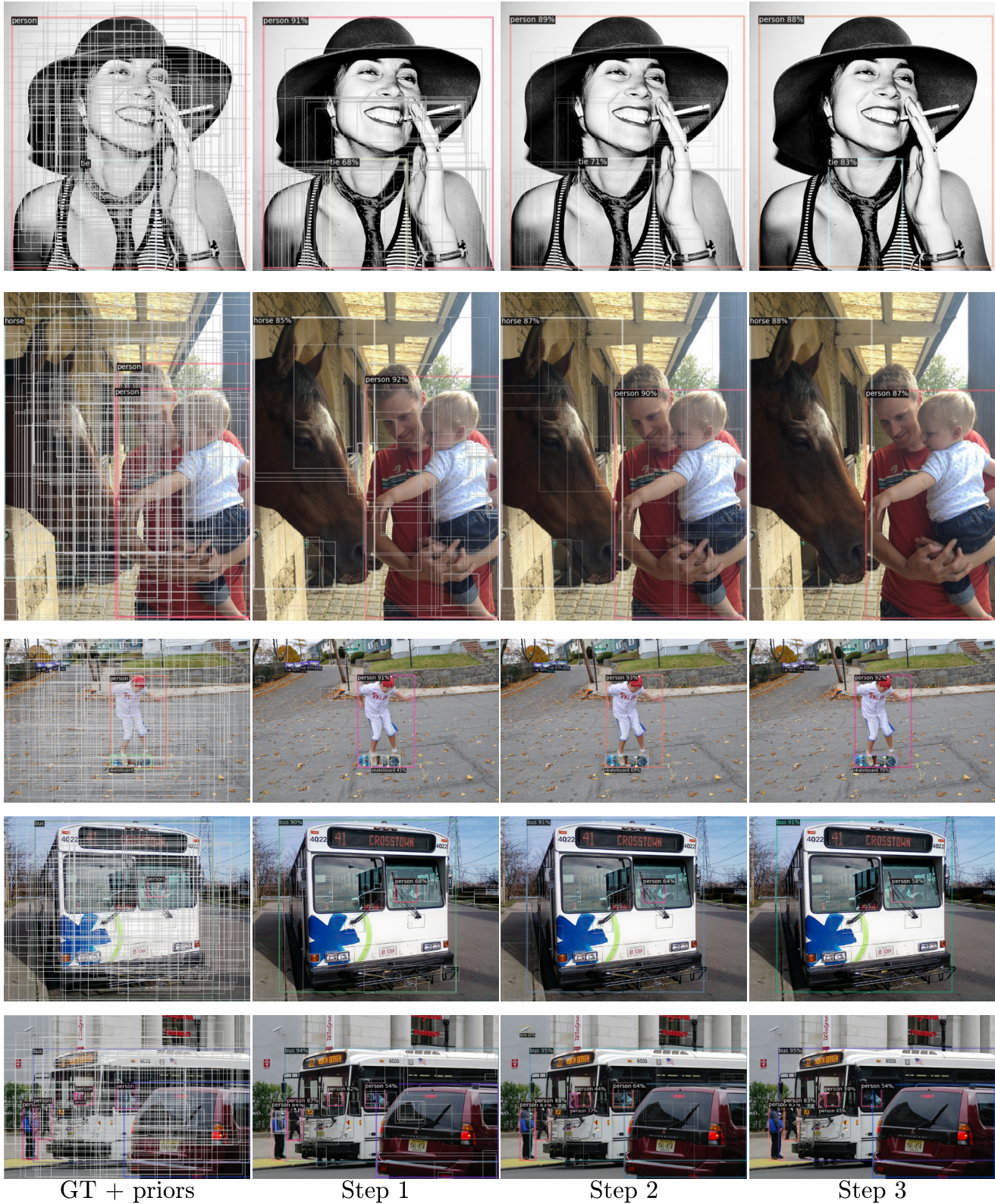


Figure 4. **Qualitative examples of FlowDet on COCO.** For each image, we show (from left to right): the input with ground-truth boxes (solid) and initial prior samples (faint), followed by the model’s predictions after 1, 2, and 3 integration steps. All examples use the same backbone, ResNet50, and inference settings as our main experiments and $N_{eval} = 100$ per image.

C. Qualitative Detection Examples

To complement the quantitative results of the main paper, we provide qualitative examples of FlowDet’s performance and failure modes in Figure 4. In particular, we illustrate how FlowDet refines detections over multiple flow steps, allowing boxes to traverse long distances and find objects even with few initial bounding box candidates. In particular, for a set of representative COCO images, we show the input with ground-truth boxes, the initial prior samples, and the model’s predictions after 1, 2, and 3 refinement steps using the same backbone and evaluation setting as in our main experiments.

As the number of steps increases, boxes are rapidly transported towards tighter, better-aligned localisations, while spurious and duplicate detections are suppressed, visually highlighting the effect of the learned flow field on detection quality. Additionally, we observe a common failure mode of NMS-based detectors in the second row of examples within Figure 4. Here, there are two overlapping ground-truth boxes of the same class, and valid detection proposals for the smaller instance are suppressed during NMS, leaving just a single bounding box as a result. It may be possible to address this using recent refinements to the labelling within COCO [31] or through exploring alternative NMS strategies, but we leave this for future work.